Heterogenized molecular (pre)catalysts for water oxidation and oxygen reduction

Ham, C.J.M. van der

3 | Activation pathways taking place at molecular copper precatalysts for the oxygen evolution reaction

Abstract

The activation processes of the complex $[Cu^{II}(bdmpza)_2]$ (bdmpza$^-$ = bis(3,5-dimethyl-1H-pyrazol-1-yl)acetate) in the water oxidation reaction were investigated using cyclic voltammetry and chronoamperometry. Two different paths wherein CuO is formed were distinguished. $[Cu^{II}(bdmpza)_2]$ can be oxidized at high potentials to form CuO, which was observed by a slight increase in catalytic current over time in chronoamperommetry. When $[Cu^{II}(bdmpza)_2]$ is initially reduced at low potentials, a more active water oxidation catalyst is generated, yielding high catalytic currents from the moment a sufficient potential is applied. This work highlights the importance of catalyst pretreatment and the choice of the experimental conditions in water oxidation catalysis using copper complexes.

"Faith and reason are like two wings on which the human spirit rises to the contemplation of truth; and God has placed in the human heart a desire to know the truth"

St. John Paul II in *Fides et Ratio*

Published in: *Catal. Today* **2016***290,* 33-38

3.1 Introduction

The water oxidation reaction has been extensively studied in the presence of homogeneous water oxidation catalysts that predominantly are based on noble metals such as ruthenium [1–3] and iridium. [4–9] In particular in case of molecular ruthenium systems bearing bipyridine type ligands, mechanistic studies have provided the community with detailed insights how water oxidation catalysis occurs. [10–12] In case of other water oxidation catalysts the true active species turned out to be metal oxide deposits that were formed from their organometallic precursors under the harsh oxidative conditions applied. [13–16] In terms of atom abundance and economic viability, complexes that are based on first row transition metals are more interesting than their second and third row counterparts, albeit such systems typically do not operate well under acidic conditions. Due to substantial faster ligand dissociation kinetics at these first row transitions metals, control over the catalyst structure is considerably more cumbersome. Nevertheless, molecular catalysts in case of manganese,[17] iron,[18–20] cobalt[21] and since very recently copper[22–30] have been reported. Especially in case of the latter, ligand exchange kinetics are fast, and consequently several papers have appeared wherein copper oxides proved to be the competent catalytic species rather than their molecular precursors.[31–35] A fruitful strategy to prevent formation of copper oxides appears to lie with multi-denticity. [29] Nevertheless, also the copper bipyridine complexes, first reported by Mayer *et al.*, appear to react exclusively via molecular sites, [22, 23] suggesting that discrimination between homogeneous versus heterogeneous catalysis is much more complex. From early cobalt polyoxometallate water oxidation chemistry the scientific community has already learned that the formation of which type of catalytic species is formed can be largely dependent on the exact reaction conditions applied, especially in case of highly dynamic systems.[36–39]

Preliminary water oxidation studies in our lab in the presence of $[Cu^{II}(bdmpza)_2]$ ($bdmpza^-$ = bis(3,5-dimethyl-1H-pyrazol-1-yl)acetate, Figure 3.1), a structure similar to the aforementioned copper bipyridine system, revealed that the observed water oxidation activity is strongly dependent on the electrochemical pretreatment of the molecular catalyst, even though the eventual catalytic experiments were carried out under the exact same conditions. In light of the discussion whether catalysis occurs at a homogeneous versus heterogeneous species and how one can

control the activity of these catalytic species, the pretreatment dependence triggered us to investigate the catalyst activation pathways of $[Cu^{II}(bdmpza)_2]$ in detail. In this contribution we discuss two independent pathways to the formation of CuO, the true active species, wherein the observed reactivity is greatly dependent on the activation path.

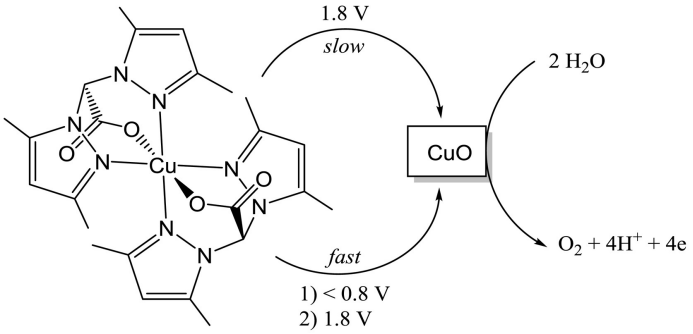

Figure 3.1: Paths of activation observed for $[Cu^{II}(bdmpza)_2]$.

3.2 Experimental

3.2.1 Materials

The bdmpzaNa ligand was synthesized by Tom van Dijkman according to literature procedure[40] and used as received. $Cu(OTf)_2$ (Alfa Aesar, 99%) was used as received.

NaOH (Merck, 99.9995%) was used as received. Electrolyte solutions were made using Millipore MilliQ water (>18.2 MΩ cm resistivity). Argon (Linde, 5.0) and hydrogen (Linde, 5.0) were used as received

3.2.2 Complex synthesis

$[Cu^{II}(bdmpza)_2]$ was obtained by dropwise addition of 0.33 mmol bdmpzaNa in 25 ml methanol to a solution of 0.33 mmol $Cu^{II}(OTf)_2$ in 25 ml methanol. After stirring for 30 minutes, part of the methanol was evaporated and diethyl ether was added to the reaction mixture to yield a blue-green precipitate overnight. The crystalline material was dried *in vacuo* and recrystallized from methanol at -20°C, yielding the complex $[Cu^{II}(bdmpza)_2]$. The infrared spectra of

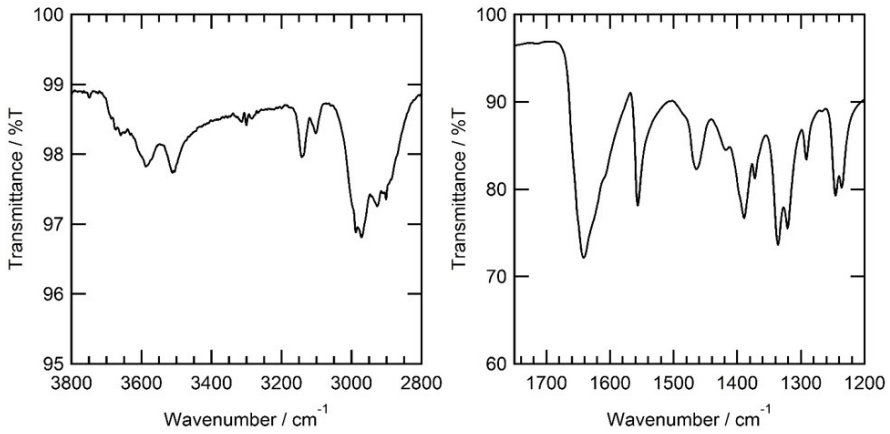

Figure 3.2: IR spectrum of $[Cu^{II}(bdmpza)_2]$, which shows characteristic vibrations: at $\tilde{\upsilon}$ = 1642 cm^{-1} (1645 cm^{-1}) [41] and $\tilde{\upsilon}$ = 1557 cm^{-1} (C-N, 1558 cm^{-1}) [41].

$[Cu^{II}(bdmpza)_2]$ are in good agreement with previous reported data (see Figure 3.2). [41] ESI MS m/z (calc):558.2 (558.2, $[M]^+$ 580.2 (580.2, $[M+Na]^+$), 612.2 (612.2, $[M+Na+MeOH]^+$).

3.2.3 Electrochemical methods

All experiments were performed on an Autolab PGSTAT 128N. All electrochemical experiments were performed in one-compartment 25 ml glass cells in a three-electrode setup, using a gold (Mateck, 99.999%) working electrode (WE). In all cases a gold wire (Mateck, 99.99%) was used as a counter electrode and all experiments were measured *versus* the reversible hydrogen electrode. The electrochemical cell was boiled twice in Millipore MilliQ water (>18.2 MΩ cm resistivity) prior to the experiment. The Au working electrode consisted of a disc (0.050 cm^2 geometric surface area) and was used in a hanging meniscus configuration. The WE was cleaned by applying 10 V between the WE and a graphite counter electrode for 30 s in a 10% H_2SO_4 solution. This was followed by dipping the WE in a 6 M HCl solution for 20 s. The electrode was flame annealed, followed by electrochemical polishing in 0.1 M $HClO_4$, while scanning between 0 and 1.75 V *versus* RHE for 200 cycles at 1 V s^{-1}. After drying the electrode *in vacuo* 5 µL of a 18 mM solution of $[Cu^{II}(bdmpza)_2]$ in ethanol was dropcasted onto the working electrode and dried in air. The electrolyte solutions were prepared from MilliQ water (>18.2 MΩ cm resistivity) and ≥99.9995%

NaOH obtained from Sigma-Aldrich.

The electrochemical quartz crystal microbalance (EQCM) experiments were performed in a 3 ml Teflon cell purchased from Autolab. As a working electrode, an Autolab EQCM electrode was used, wherein a 200 nm gold layer (0.35 cm^2) was deposited on a quartz crystal. Since the hydrogen bubbles of the RHE reference electrode disturbed the frequency during the EQCM measurements, a Pd/H_2 reference electrode was prepared by applying a potential of -4.0 V between the Pd wire and a platinum counter electrode for approximately 10 min. Prior to the experiment the potential of the Pd/H_2 electrode relative to the RHE was determined. All EQCM data were corrected to the RHE scale. The sensitivity coefficient (c_f) was determined to be 1.26×10^{-8} µg cm^{-2} Hz^{-1}, *c.f.* Figure 2.3 in chapter 2.

During the online electrochemical mass spectrometry (OLEMS) measurements the gaseous products formed at the working electrode were collected via a hydrophobic tip (KEL-F with a porous Teflon plug) in close proximity to the surface of the working electrode and analyzed in a Pfeiffer QMS 200 mass spectrometer. An Ivium A06075 potentiostat was used in combination with the OLEMS experiments. A detailed description of the OLEMS setup is available elsewhere. [42]

3.2.4 XPS

The XPS measurements were carried out with a Thermo Scientific K-Alpha, equipped with a monochromatic small-spot X-ray source and a 180° double focusing hemispherical analyzer with a 128-channel detector. Spectra were obtained using an aluminium anode (Al Kα = 1486.6 eV) operating at 72 W and a spot size of 400µm. Survey scans were measured at a constant pass energy of 200 eV and region scans at 50 eV. The background pressure was 2×10^{-8} mbar and during measurement 4 x 10^{-7} mbar Argon because of charge compensation.

Samples for XPS were prepared by chronoamperometry in 0.1 M NaOH at pH 13, using 0.8 cm^2 pyrolitic graphite discs as working electrodes. Prior to use, the electrodes were sanded with waterproof 2500 grit sandpaper. A total amount of 180 nmol $[Cu^{II}(bdmpza)_2]$ was dropcasted onto the electrodes and the discs were used in a hanging meniscus configuration.

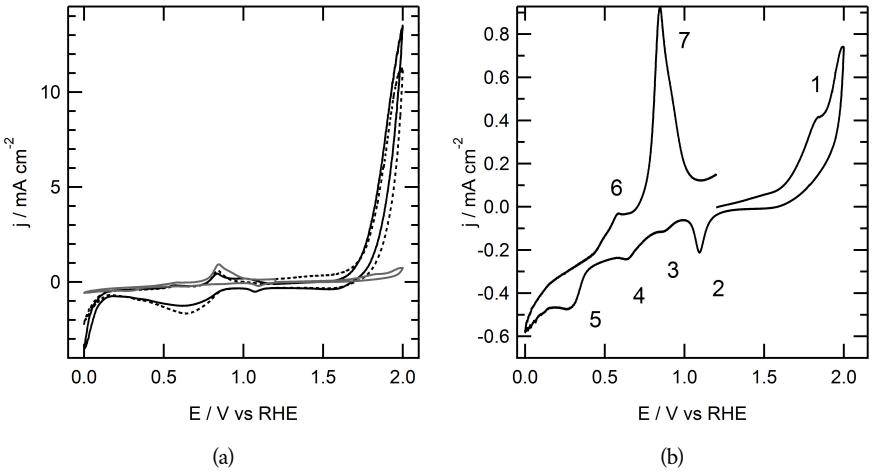

Figure 3.3: (a) The first three scans of a cyclic voltammetry experiment of $[Cu^{II}(bdmpza)_2]$ in 0.1 M NaOH at a 100 mV s^{-1} scan rate. The first scan of the cyclic voltammetry (grey line) is depicted in magnified view separately (b) from the 2nd (dotted black line) and 3rd scan (solid black line).

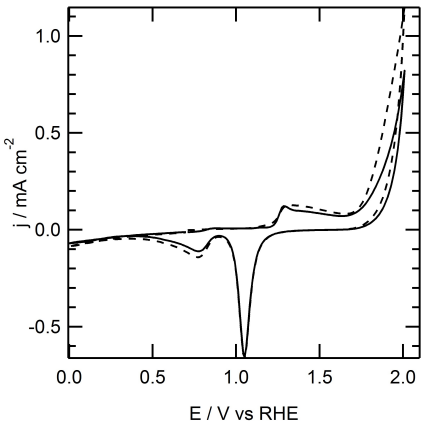

Figure 3.4: First (dotted line) and second (solid line) scan of a cyclic voltammogram of a Au WE in 0.1 M NaOH electrolyte solution at a scan rate of 100 mV s^{-1}.

3.3 Results

The bdmpza$^-$ ligands of [Cu^{II}(bdmpza)$_2$] are centrosymmetrically arranged around the copper ion, forming a trans-CuN_4O_2 complex, wherein the copper site is coordinatively saturated.[41] However, it is not unprecedented that one of the ligand arms of bdmpza$^-$ dissociates in favor of coordination of water,[43] providing an entry into catalysis at a molecular species. The redox chemistry of [Cu^{II}(bdmpza)$_2$] was explored by dropcasting the complex onto a gold working electrode (WE). Figure 3.3 shows the cyclic voltammogram of 90 nmol [Cu^{II}(bdmpza)$_2$] dropcasted onto a 0.050 cm^2 (geometric surface area) gold electrode in a 0.1 M aqueous NaOH solution at pH 13. The experiment was started at 1.2 V *versus* RHE and scanned towards positive potentials initially. In the first scan relatively little catalytic current is observed, which contrasts the second and third scans. Scanning the potential up to 2.0 V *versus* RHE resulted in a small peak (designated 1 in Figure 3.3b) in the cyclic voltammogram, which does not exceed the current displaying that of a blank gold electrode under the same conditions (see Figure 3.4).

While starting above 1.2 V *versus* RHE and scanning into a positive direction first or scanning in negative direction immediately does not result in changes in the reduction chemistry. Below 1.2 V a series of sharp reduction peaks (2-5 in Figure 3.3b) can be observed that lie on top of a

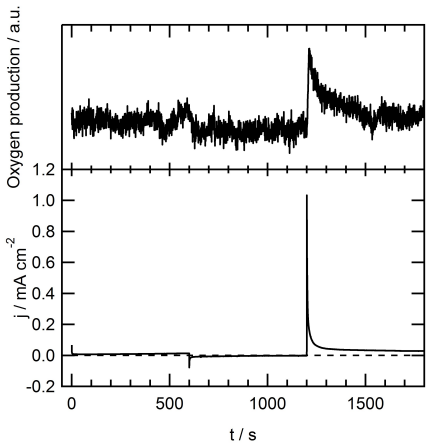

Figure 3.5: Chronoamperometry of 360 nmol $[Cu^{II}(bdmpza)_2]$ dropcasted onto a 0.72 cm^2 gold electrode (geometrical surface area) in 0.1 M NaOH. The potential was set at 2.0 V *versus* RHE for 600 seconds, then set to 0.0 V for another 600 seconds and then returned to 2.0 V for the last 600 seconds (bottom panel). The evolution of dioxygen was followed simultaneously using OLEMS (top panel).

broad negative baseline current that starts roughly at 0.8 V *versus* RHE. The negative baseline current continues upon scanning into the positive direction until 0.8 V after which a very sharp oxidative peak (7) is observed at 0.9 V *versus* RHE. With an onset of roughly 1.6 V *versus* RHE a substantial catalytic wave is observed in the cyclic voltammetry that greatly exceeds the oxidative current that was observed in the first scan. When an initial starting potential was selected below 0.8 V *versus* RHE, such a catalytic current can already be observed at the very first oxidative scan, suggesting it is triggered by an initial reduction of $[Cu^{II}(bdmpza)_2]$. In the second reductive scan a broad feature at 0.5 V *versus* RHE is observed followed by a catalytic reductive current with an onset at 0.2 V *versus* RHE. This latter catalytic feature is most likely due to reduction of dioxygen that is formed above 1.7 V *versus* RHE in the second scan. From here on the redox features in the cyclic voltammogram do not further change upon potential cycling. The catalytic current does increase somewhat from scan 2 to 3, indicating that still more active water oxidation sites are formed on the WE.

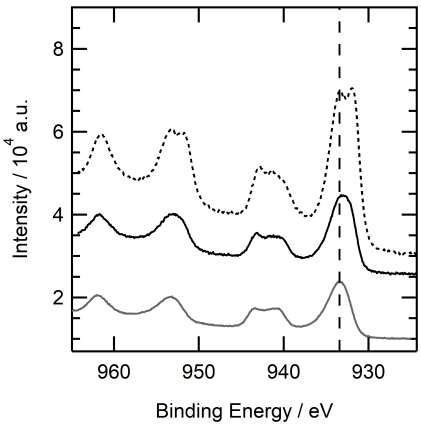

Figure 3.6: *Ex situ* XPS spectra taken after dropcasting 180 nmol $[Cu^{II}(bdmpza)_2]$ onto 0.88 cm^2 pyrolitic disc and applying 2.0 V for 10 minutes (black dotted line), applying 0 V for 10 minutes followed by 10 minutes of applying 2.0 V (black solid line). The grey line is benchmark CuO, while the vertical dotted line is at 933.4, indicating the peak for CuO.

The displayed catalytic activity in the presence of $[Cu^{II}(bdmpza)_2]$ was further evaluated by chronoamperometry experiments using both gold (Figure 3.5) and pyrolytic graphite electrodes. In this series of experiments 1.2 V *versus* RHE was selected as a standby potential as no oxidative or reductive currents were observed at this potential in the first scan of the voltammogram of $[Cu^{II}(bdmpza)_2]$. On gold an initial current of 7 μA cm^{-2} was observed after 120 seconds of amperometry at 2.0 V that steadily increased to 13 μA cm^{-2} after 30 minutes (Figure 3.5). This suggests that some activation of $[Cu^{II}(bdmpza)_2]$ to a (more) active catalytic species takes place under these oxidative conditions. In line with the oxidative current observed in the amperometry, online electrochemical mass spectrometry (OLEMS) data do show formation of some dioxygen over the course of time (Figure 3.5, top panel).

X-ray photoelectron spectroscopy of $[Cu^{II}(bdmpza)_2]$ dropcasted on a pyrolytic graphite electrode that was kept at 2.0 V *versus* RHE for 10 minutes shows two independent signals in the binding energy region of the 2p electrons of copper at 931.1 and 933.3 eV (see Figure 3.6. The low binding energy peak (931.3 eV) can be due to either Cu metal or a Cu(I) species, such as

Cu_2O. The Cu LMM Auger peaks exclude the presence of metallic Cu (which has a distinct peak at 565,5 eV), and, interestingly, also that of $Cu(OH)_2$(which has a peak at 570.4 eV).[44] The signal at 933.3 eV is similar to that of CuO for which we find a binding energy of 933.4 eV (slightly higher values have been reported in literature: *i.e.* 933.9 eV, [34] 933.7 eV, [45] 933.8 eV [46]). The shake-up structure is mostly characteristic of CuO, except for the small but visible feature on the high binding energy side (about 942 eV), which is also present in the spectrum of Cu_2O. Hence we interpret the *ex situ* XPS measurement of $[Cu^{II}(bdmpza)_2]$ kept at 2.0 V *versus* RHE for 10 minutes to a mixture of Cu(I) and Cu(II) oxides, while the spectra show no evidence for Cu metal nor $Cu(OH)_2$. Apparently $[Cu^{II}(bdmpza)_2]$ slowly converts to CuO at 2.0 V *versus* RHE. Since CuO is a known water oxidation catalyst[33, 34, 47] and the catalytic activity increases upon prolonged electrolysis it seems likely that CuO is responsible for most, if not all, catalytic current. In fact at this point we have no reason to believe that any of the observed catalytic activity should be ascribed to the $[Cu^{II}(bdmpza)_2]$ species itself.

When the potential after the initial amperometry experiment at 2.0 V is set at 0.0 V for 10 minutes and then placed back at 2.0 V *versus* RHE, a considerably higher catalytic current is observed. This is in line with OLEMS data at this stage, which shows that a considerable amount of dioxygen is produced (Figure 3.5, top panel). After 60 seconds a current of 56 μA cm^{-2} was recorded that slowly decreased to 28 μA cm^{-2}. Even higher catalytic currents are obtained when $[Cu^{II}(bdmpza)_2]$ is immediately reduced at 0 V and then brought to 2.0 V. X-ray photoelectron spectroscopy now only shows a single peak at 933.3 eV suggesting that full conversion to CuO has taken place. The decrease of the catalytic current upon prolonged electrolysis is most likely due to depletion of Cu^{2+} from the electrode under these conditions. It is likely that upon reduction $[Cu^{II}(bdmpza)_2]$ converts to metallic Cu(0) at the electrode interface that in turn is oxidized to CuO. For several related systems conversion of molecular species to Cu(0) has been observed in relation to the catalytic hydrogen evolution reaction.[48–50]

From the cyclic voltammetry in Figure 3.3 it was observed that the electrochemical reduction of $[Cu^{II}(bdmpza)_2]$ has a great influence on the current observed in the oxidative regime and is believed to proceed via initial formation of metallic copper. An electrochemical quartz crystal microbalance (EQCM) in combination with cyclic voltammetry is a powerful tool to gain insight into adsorption processes taking place on the electrode. In these studies roughly 180

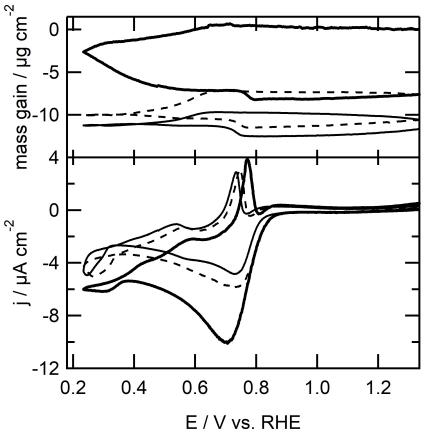

Figure 3.7: Electrochemistry of $[Cu^{II}(bdmpza)_2]$ combined with a quartz crystal microbalance showing the loss of mass of the electrode (top panel) during cyclic voltammetry (bottom panel) in a 0.1 M aqueous NaOH solution of pH 13. E_{start} = 1.3 V, scan rate = 1 mV s^{-1}.

nmol $[Cu^{II}(bdmpza)_2]$ in EtOH was dropcasted onto the EQCM electrode. Figure 3.7 shows the EQCM of $[Cu^{II}(bdmpza)_2]$ between 1.3 and 0.2 V *versus* RHE. The bottom panel shows the potential — current relationship from the CV, whereas the top panel shows the corresponding mass change of the quartz crystal, determined from the change in oscillation frequency of the quartz crystal simultaneously with the cyclic voltammetry experiment. At a scan rate of 1 mV s^{-1} a broad and clearly visible reduction peak is observed with an onset of 0.7 *versus* RHE, due to reduction of $[Cu^{II}(bdmpza)_2]$ to Cu(0). The features observed in the cyclic voltammetry upon reduction leading to formation of copper are strongly scan rate dependent. Similar to the cyclic voltammetry depicted in Figure 3.3b, a negative baseline is observed in both negative and positive scan. In addition to reduction of $[Cu^{II}(bdmpza)_2]$, this in part may be due to reduction of some dioxygen that leaks into the Teflon EQCM cell. The top panel of Figure 3.7 shows that the initial mass of the electrode does not change upon scanning the potential from 1.3 to 0.7 V *versus* RHE. Beyond the onset of the reduction wave at 0.7 V *versus* RHE in the cyclic voltammogram, the mass of the crystal starts to decrease, indicating that desorption of material from the electrode takes place. This mass decrease continues in the positive going scan and reaches a plateau

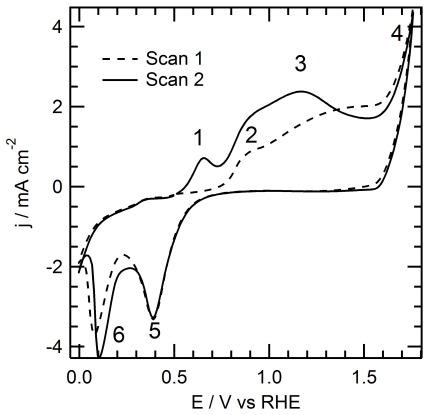

Figure 3.8: Cyclic voltammogram of a polycrystalline Cu electrode at 100 mV s^{-1} in 0.1 M aqueous NaOH solution (pH 13). The experiment is started at 0.5 V versus RHE and scanned towards positive potentials first.

at 0.4 V *versus* RHE. The sharp oxidation peak observed at 0.8 V *versus* RHE is considerably less dependent on the scan rate. This is most likely a stripping peak,[51] illustrated by a small and abrupt decrease in mass. The second and third scan show considerably less current and smaller mass changes than the first scan and is in agreement with a high conversion of $[Cu^{II}(bdmpza)_2]$ to metallic copper at this stage. In Figure 3.7, a total charge of 8.5 mC has passed through the WE to reduce $[Cu^{II}(bdmpza)_2]$, which equals a total of 88 nmol electrons. A larger amount of 180 nmol $[Cu^{II}(bdmpza)_2]$ was dropcasted onto the gold electrode, but it proved difficult to exclude large amounts of material from ending up on the quartz rather than on the gold surface which is electrochemically active. Moreover some of the charge flow may be due to reduction of dioxygen as it proved to be difficult to exclude air leaking into the Teflon EQCM cell. Nevertheless these numbers are in line with a considerable part of the dropcasted material to be reduced to copper in the EQCM experiment and agree with full conversion of $[Cu^{II}(bdmpza)_2]$ to take place during prolonged amperometry at 0.0 V *versus* RHE.

The EQCM data in Figure 3.7 shows that relatively little ligand ($\sim$75 nmol bdmpza equaling 21 % of dropcasted bdmpza) is lost from the electrode interface during the reduction of

$[Cu^{II}(bdmpza)_2]$ to Cu(0). Also the amount of copper lost to the solution at the copper stripping peak at 0.8 V *versus* RHE is limited (after three scans $\sim$ 70 nmol Cu, 38 % of all dropcasted copper).

In the cyclic voltammetry of polycrystalline copper a small oxidation wave is observed at 0.6 V *versus* RHE that is ascribed to oxidation of Cu(0) to Cu_2O (Figure 3.8, signal 1).[51] A very similar oxidation wave is observed at 0.6 V in case of deposited $[Cu^{II}(bdmpza)_2]$ (Figures 3.3 and 3.7). Further oxidation to CuO, however, is considerably more facile in case of deposited $[Cu^{II}(bdmpza)_2]$ compared to polycrystalline copper, which shows broad features (signals 2 and 3 in Figure 3.8) as the result of oxidation of different crystal domains.[51–53] The copper deposit obtained from $[Cu^{II}(bdmpza)_2]$ only shows a small and very sharp oxidation wave (Figure 3.3b, signal 7). We have been unable to reproduce these electrochemical features of using other sources of copper, including copper oxide nanoparticles, $Cu(OTf)_2$ and a polycrystalline copper electrode (see Figure 3.8). In all these cases copper is considerably easier removed from the electrode surface compared to samples of $[Cu^{II}(bdmpza)_2]$. In line with the remarkable stability of the copper catalyst obtained from $[Cu^{II}(bdmpza)_2]$ compared to other sources of copper, also the observed catalytic current is more persistent and significantly higher. It appears that the bdmpza ligand has clear effect on the stability of the copper particles that are formed, and seems to prevent solvation of Cu^{2+} upon reoxidation of copper to the +II oxidation state. In line with such a hypothesis the presence of concentrated solutions of carbonate[54] and especially borate[34, 55] have a dramatic influence on the stability and therefore activity of copper deposits under oxidative conditions. It seems that similar to coordinating anions, the $bdmpza^-$ ligand has a stabilizing effect on copper oxide *versus* solvation, thereby posing an interesting application of the use of organic ligands and/or additives in heterogeneous water oxidation chemistry.

3.4 Conclusions

Two paths haven been identified wherein $[Cu^{II}(bdmpza)_2]$ is converted to CuO, which is the true active species in the water oxidation reaction (Figure 3.9). Under oxidative conditions the complex $[Cu^{II}(bdmpza)_2]$ slowly converts to CuO and leads to moderate activity only. Initial reduction of $[Cu^{II}(bdmpza)_2]$ below 0.8 V *versus* RHE leads to initial formation of Cu(0), which ultimately converts to CuO under catalytic conditions. This path leads to a substantial higher cat-

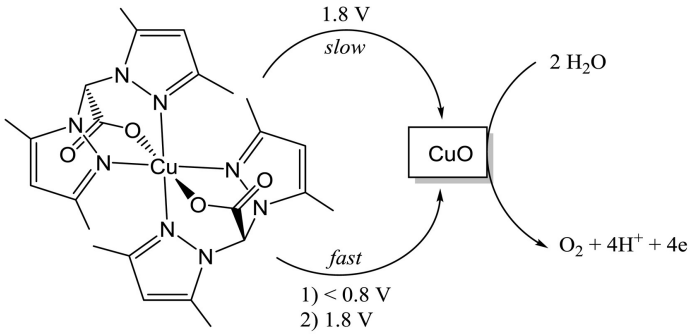

Figure 3.9: Activation pathways of $[Cu^{II}(bdmpza)_2]$ towards CuO, the active water oxidation catalyst.

alytic activity under the conditions explored. One therefore has to be very careful which standby and/or start potential is selected prior to catalytic water oxidation mediated by molecular copper complexes, as these settings may have a dramatic effect on the displayed catalytic activity as illustrated above. Also the $bdmpza^-$ ligand plays an important role in the observed catalytic activity, since dropcasting various other copper sources results in mediocre stability and activity. Clearly one cannot use such alternative copper sources convincingly as a control for the formation of active CuO nanoparticles. The precise mechanism wherein $bdmpza^-$ influences the catalytic activity is not well understood at present.

Acknowledgments

The authors gratefully acknowledge dr. Tom van Dijkman and prof. dr. Elisabeth Bouwman for supplying the bdmpzaNa ligands used in this work. This work was financially supported by the ERC (StG 637556).

References

(1) Duan, L.; Bozoglian, F.; Mandal, S.; Stewart, B.; Privalov, T.; Llobet, A.; Sun, L. *Nat. Chem.* **2012**, *4*, 418–423.

(2) Matheu, R.; Ertem, M. Z.; Benet-Buchholz, J.; Coronado, E.; Batista, V. S.; Sala, X.; Llobet, A. *J. Am. Chem. Soc.* **2015**, *137*, 10786–10795.

(3) Concepcion, J. J.; Jurss, J. W.; Norris, M. R.; Chen, Z.; Templeton, J. L.; Meyer, T. J. *Inorg. Chem.* **2010**, *49*, 1277–1279.

(4) Diaz-Morales, O.; Hersbach, T. J. P.; Hetterscheid, D. G. H.; Reek, J. N. H.; Koper, M. T. M. *J. Am. Chem. Soc.* **2014**, *136*, 10432–10439.

(5) Lalrempuia, R.; McDaniel, N. D.; Müller-Bunz, H.; Bernhard, S.; Albrecht, M. *Angew. Chem. Int. Ed.* **2010**, *49*, 9765–9768.

(6) Bucci, A.; Savini, A.; Rocchigiani, L.; Zuccaccia, C.; Rizzato, S.; Albinati, A.; Llobet, A.; Macchioni, A. *Organometallics* **2012**, *31*, 8071–8074.

(7) Sheehan, S. W.; Thomsen, J. M.; Hintermair, U.; Crabtree, R. H.; Brudvig, G. W.; Schmuttenmaer, C. A. *Nat. Commun.* **2015**, *6*, 6469.

(8) Blakemore, J. D.; Schley, N. D.; Balcells, D.; Hull, J. F.; Olack, G. W.; Incarvito, C. D.; Eisenstein, O.; Brudvig, G. W.; Crabtree, R. H. *J. Am. Chem. Soc.* **2010**, *132*, 16017–16029.

(9) Hetterscheid, D. G. H.; van der Ham, C. J. M.; Diaz-Morales, O.; Verhoeven, M. W. G. M.; Longo, A.; Banerjee, D.; Niemantsverdriet, J. W.; Reek, J. N. H.; Feiters, M. C. *Phys. Chem. Chem. Phys.* **2016**, *18*, 10931–10940.

(10) Nyhlén, J.; Duan, L.; Åkermark, B.; Sun, L.; Privalov, T. *Angew. Chem. Int. Ed.* **2010**, *49*, 1773–1777.

(11) Concepcion, J. J.; Tsai, M.-K.; Muckerman, J. T.; Meyer, T. J. *J. Am. Chem. Soc.* **2010**, *132*, 1545–1557.

(12) Chen, Z.; Concepcion, J. J.; Hu, X.; Yang, W.; Hoertz, P. G.; Meyer, T. J. *P. Natl, Acad. Sci. U.S.A.* **2010**, *107*, 7225–9.

(13) Fukuzumi, S.; Hong, D. C. *Eur. J. Inorg. Chem.*. **2014**, 645–659.

(14) Limburg, B.; Bouwman, E.; Bonnet, S. *Coordin. Chem. Rev.* **2012**, *256*, 1451–1467.

(15) Junge, H.; Marquet, N.; Kammer, A.; Denurra, S.; Bauer, M.; Wohlrab, S.; Gärtner, F.; Pohl, M.-M.; Spannenberg, A.; Gladiali, S.; Beller, M. *Chem. Eur. J.* **2012**, *18*, 12749–12758.

(16) Blakemore, J. D.; Schley, N. D.; Olack, G. W.; Incarvito, C. D.; Brudvig, G. W.; Crabtree, R. H. *Chem. Sci.* **2011**, *2*, 94–98.

(17) Limburg, J.; Vrettos, J. S.; Liable-Sands, L. M.; Rheingold, A. L.; Crabtree, R. H.; Brudvig, G. W. *Science* **1999**, *283*, 1524–1527.

(18) Lloret-Fillol, J.; Codolà, Z.; Garcia-Bosch, I.; Gómez, L.; Pla, J. J.; Costas, M. *Nat. Chem.* **2011**, *3*, 807–813.

(19) Kottrup, K. G.; Hetterscheid, D. G. H. *Chem. Commun.* **2016**, *52*, 2643–2646.

(20) Ellis, W. C.; McDaniel, N. D.; Bernhard, S.; Collins, T. J. *J. Am. Chem. Soc.* **2010**, *132*, 10990–10991.

(21) Wasylenko, D. J.; Ganesamoorthy, C.; Borau-Garcia, J.; Berlinguette, C. P. *Chem. Commun.* **2011**, *47*, 4249.

(22) Barnett, S. M.; Goldberg, K. I.; Mayer, J. M. *Nat. Chem.* **2012**, *4*, 498–502.

(23) Gerlach, D. L.; Bhagan, S.; Cruce, A. A.; Burks, D. B.; Nieto, I.; Truong, H. T.; Kelley, S. P.; Herbst-Gervasoni, C. J.; Jernigan, K. L.; Bowman, M. K.; Pan, S.; Zeller, M.; Papish, E. T. *Inorg. Chem.* **2014**, *53*, 12689–12698.

(24) Pap, J. S.; Szyrwiel, L.; Srankó, D.; Kerner, Z.; Setner, B.; Szewczuk, Z.; Malinka, W. *Chem. Commun.* **2015**, *51*, 6322–6324.

(25) Zhang, T.; Wang, C.; Liu, S.; Wang, J.-L.; Lin, W. *J. Am. Chem. Soc.* **2014**, *136*, 273–281.

(26) Su, X.-J.; Gao, M.; Jiao, L.; Liao, R.-Z. Z.; Siegbahn, P. E. M.; Cheng, J.-P.; Zhang, M.-T. *Angew. Chem. Int. Ed.* **2015**, *54*, 4909–4914.

(27) Zhang, M.-T.; Chen, Z.; Kang, P.; Meyer, T. J. *J. Am. Chem. Soc.* **2013**, *135*, 2048–2051.

(28) Chen, Z.; Meyer, T. J. *Angew. Chem. Int. Edit.* **2013**, *52*, 700–703.

(29) Garrido-Barros, P.; Funes-Ardoiz, I.; Drouet, S.; Benet-Buchholz, J.; Maseras, F.; Llobet, A. *J. Am. Chem. Soc.* **2015**, *137*, 6758–6761.

(30) Coggins, M. K.; Zhang, M.-T.; Chen, Z.; Song, N.; Meyer, T. J. *Angew. Chem. Int. Ed.* **2014**, *53*, 12226–12230.

(31) Li, T.-T.; Cao, S.; Yang, C.; Chen, Y.; Lv, X.-J.; Fu, W.-F. *Inorg. Chem.* **2015**, *54*, 3061–3067.

(32) Liu, X.; Jia, H.; Sun, Z.; Chen, H.; Xu, P.; Du, P. *Electrochem. Commun.* **2014**, *46*, 1–4.

(33) Liu, X.; Cui, S.; Sun, Z.; Du, P. *Electrochim. Acta* **2015**, *160*, 202–208.

(34) Yu, F.; Li, F.; Zhang, B.; Li, H.; Sun, L. *ACS Catal.* **2015**, *5*, 627–630.

(35) Liu, X.; Cui, S.; Qian, M.; Sun, Z.; Du, P. *Chem. Commun.* **2016**, *52*, 5546–5549.

(36) Folkman, S. J.; Kirner, J. T.; Finke, R. G. *Inorg. Chem.* **2016**, *55*, 5343–5355.

(37) Stracke, J. J.; Finke, R. G. *J. Am. Chem. Soc.* **2011**, *133*, 14872–14875.

(38) Stracke, J. J.; Finke, R. G. *ACS Catal.* **2013**, *3*, 1209–1219.

(39) Vickers, J. W.; Lv, H. J.; Sumliner, J. M.; Zhu, G. B.; Luo, Z.; Musaev, D. G.; Geletii, Y. V.; Hill, C. L. *J. Am. Chem. Soc.* **2013**, *135*, 14110–14118.

(40) Burzlaff, N.; Hegelmann, I.; Weibert, B. *J. Organomet. Chem.* **2001**, *626*, 16–23.

(41) Kozlevcar, B.; Gamez, P.; de Gelder, R.; Driessen, W. L.; Reedijk, J. *Eur. J. Inorg. Chem.* **2003**, 47–50.

(42) Wonders, A. H.; Housmans, T. H. M.; Rosca, V.; Koper, M. T. M. *J. Appl. Electrochem.* **2006**, *36*, 1215–1221.

(43) Kozlevčar, B.; Golobic, A.; Gamez, P.; Koval, I. A.; Driessen, W. L.; Reedijk, J. *Inorg. Chim. Acta* **2005**, *358*, 1135–1140.

(44) Waechtler, T.; Oswald, S.; Roth, N.; Jakob, A.; Lang, H.; Ecke, R.; Schulz, S. E.; Gessner, T.; Moskvinova, A.; Schulze, S.; Hietschold, M. *J. Electrochem. Soc.* **2009**, *156*, H453.

(45) Durando, M.; Morrish, R.; Muscat, A. J. *J. Am. Chem. Soc.* **2008**, *130*, 16659–16668.

(46) Moulder, J. F.; Stickle, W. F.; Sobol, P. E.; Bomben, K. D. Handbook of X-ray Photoelectron Spectroscopy., 1995.

(47) Liu, X.; Cui, S.; Sun, Z.; Ren, Y.; Zhang, X.; Du, P. *J. Phys. Chem. C* **2016**, *120*, 831–840.

(48) Kugler, M.; Scholz, J.; Kronz, A.; Siewert, I. *Dalton T.* **2016**, *45*, 6974–6982.

(49) Liu, X.; Zheng, H.; Sun, Z.; Han, A.; Du, P. *ACS Catal.* **2015**, *5*, 1530–1538.

(50) Liu, X.; Cui, S.; Sun, Z.; Du, P. *Chem. Commun.* **2015**, *51*, 12954–12957.

(51) Giri, S. D.; Sarkar, a. *J. Electrochem. Soc.* **2016**, *163*, I1252–I1259.

(52) Ambrose, J.; Barradas, R. G.; W., S. D. *J. Electroanal. Chem.* **1973**, *47*, 65–80.

(53) Droog, J. M. M.; Alderliesten, C. A.; Alderliesten, P. T.; Bootsma, G. A. *J. Electroanal. Chem.* **1980**, *111*, 61–70.

(54) Du, J.; Chen, Z.; Ye, S.; Wiley, B. J.; Meyer, T. J. *Angew. Chem. Int. Ed.* **2015**, *54*, 2073–2078.

(55) Shi, Y.; Gimbert-Surinach, C.; Han, T.; Berardi, S.; Lanza, M.; Llobet, A. *ACS Appl. Mater. Inter.* **2016**, *8*, 696–702.